Available online at www.sciencedirect.com

ScienceDirect

Ceramics International 40 (2014) 2691–2696

CERAMICS INTERNATIONAL

www.elsevier.com/locate/ceramint

Efficient visible-light photocatalysts from Gd–La codoped TiO_2 nanotubes

Yuchao Chai[a,1], Lin Lin[b,*,1], Ke Zhang[b], Bin Zhao[b], Dannong He[a,b]

[a]School of Materials Science and Engineering, Shanghai JiaoTong University, 200240 Shanghai, PR China
[b]National Engineering Research Center for Nanotechnology, 200241 Shanghai, PR China

Received 13 September 2013; received in revised form 12 October 2013; accepted 12 October 2013
Available online 21 October 2013

Abstract

Robust visible-light Gd–La codoped TiO_2 nanotubes were successfully synthesized via an ultrasonic hydrothermal method and the photocatalytic activities were evaluated by photodegrading Rhodamine B (RB). The calcined Gd–La codoped TiO_2 nanotubes have significantly enhanced photocatalytic activities than the uncalcined ones. The La^{3+} and Gd^{3+} in the lattices of rare earth oxides may be substituted by Ti^{4+}, creating abundant oxygen vacancies and surface defects for electron trapping and dye adsorption, accelerating the separation of photogenerated electron–hole pairs and RB photodegradation. The formation of an excitation energy level below the conduction band of TiO_2 from the binding of electrons and oxygen vacancies decreases the excitation energy of Gd–La codoped TiO_2 nanotubes, resulting in robust photocatalysts. The results suggest that Gd–La codoped TiO_2 nanotubes calcined at 500 °C are very promising for enhancing the photocatalytic activity of photocatalysts in visible-light region.

Keywords: Photocatalysts; Rare earth oxides; TiO_2 nanotubes; Semiconductors

1. Introduction

One-dimensional (1D) semiconductor nanostructures have been at the heart of current nanoscience and nanotechnology and have led to growing interest in the field of environmental and energy applications [1–5]. Among multitudinous 1D semiconductors, titania (TiO_2) nanotubes with a wide bandgap of 3.2 eV have been extensively studied as photocatalysts and energy harvesting [6,7]. However, the main drawbacks of TiO_2 are the fast recombination of photogenerated electron–hole pairs and UV-only response due to its wide bandgap, which limit TiO_2 commercial applications [8]. By addressing these issues, many attempts have been devoted to enhance the photocatalytic activity of TiO_2 by doping rare earth elements into TiO_2 nanostructures, resulting in either enhancement of photogenerated charge separation or extension of light absorption span [9]. These two aspects may be simultaneously realized by codoping TiO_2 nanostructures with bi-rare earth elements.

In search for more robust photocatalysts, here we report the study of Gd–La codoped TiO_2 nanotubes as efficient photocatalysts for Rhodamine B (RB) photodegradation. To the best of our knowledge, there is no literature about the La and Gd codoped TiO_2 nanotubes as photocatalysts. Different from the traditional approaches for the excitation enhancement of TiO_2 photocatalysts, the abundant oxygen vacancies can bind with electrons to create excitation energy below the conduction band of TiO_2, leading to an efficient excitation under visible-light irradiation.

2. Experimental

2.1. Synthesis of Gd–La codoped TiO_2 nanotubes

Gd–La codoped TiO_2 nanotubes were synthesized via an ultrasonic hydrothermal method. In details, a mixture of P25 TiO_2 nanoparticles and NaOH was made by agitating 1 g of P25 TiO_2 nanoparticles (purchased from Degussa P25 with an average diameter of 30 nm, the ratio of rutile/anatase is 3/7 with average diameter of 30 nm) and 50 ml of 10 M NaOH

*Corresponding author. Tel.: +86 21 34291286; fax: +86 21 34291125.
E-mail addresses: linlin21023@163.com (L. Lin), hdnbill@sh163.net (D. He).
[1]Joint first co-authors.

0272-8842/$ - see front matter © 2013 Elsevier Ltd and Techna Group S.r.l. All rights reserved.
http://dx.doi.org/10.1016/j.ceramint.2013.10.054

aqueous solution. Under ultrasonic vibration for 1h, lanthanum nitrate (molar ratio of La to Ti is 0.015:1) and gadolinium nitrate (molar ratio of Gd to Ti is 0.004:1) were added to the above mixture and then sealed in a Teflonlined stainless autoclave followed by heating at 110 °C for 24 h. The precipitates were filtrated and thoroughly rinsed by 0.1 M HCl aqueous solution and deionized water until the pH of filtrate is around 7.0. After being vacuum dried at 80 °C, the semi-products were calcined at

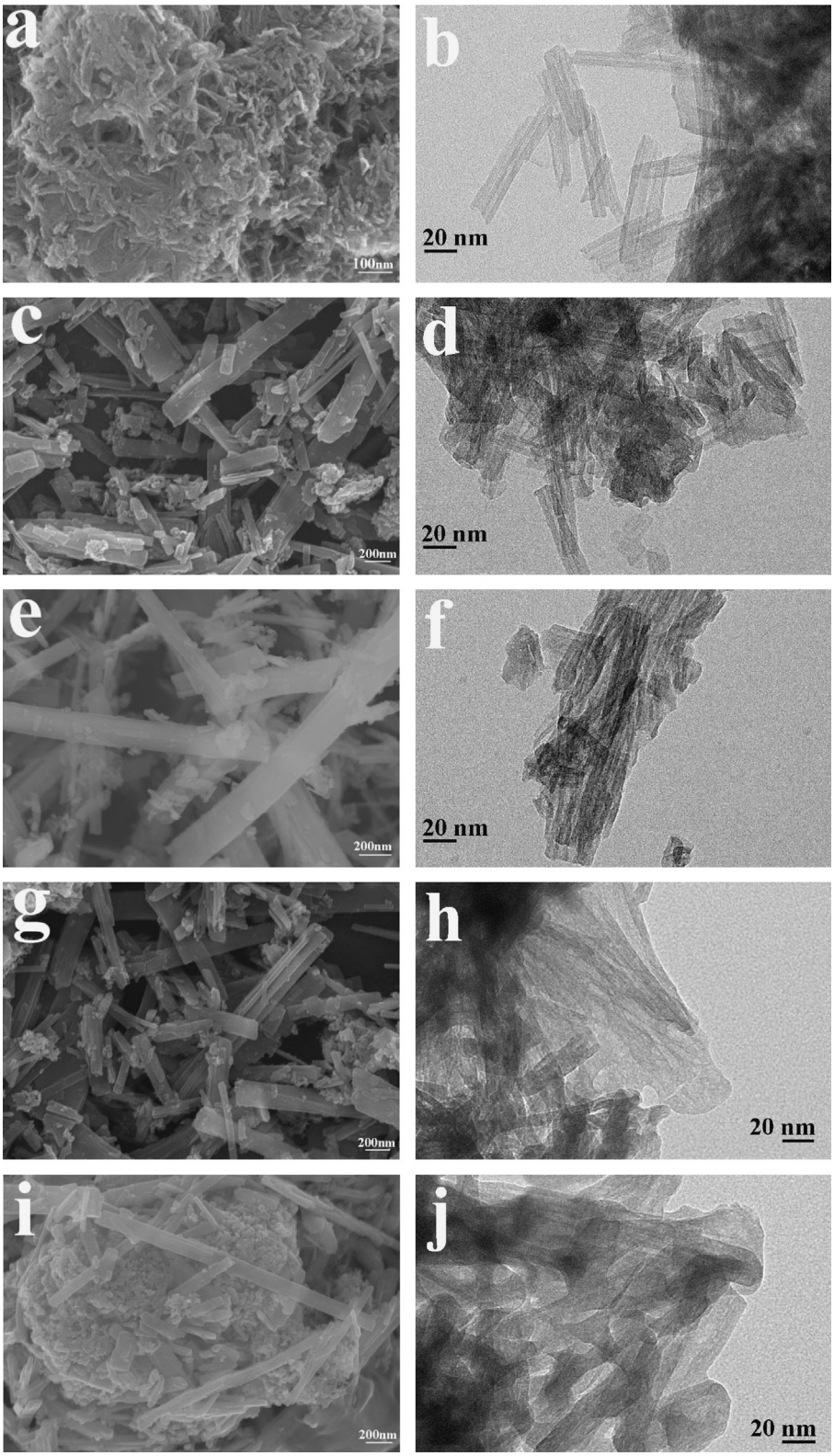

Fig. 1. SEM and TEM images of (a and b) uncalcined Gd–La codoped TiO_2 nanotubes, and Gd–La codoped TiO_2 nanotubes calcined at (c and d) 300 °C, (e and f) 400 °C, (g and h) 500 °C, and (i and j) 600 °C. The scale bars in the TEM images were all 20 nm.

300, 400, 500, and 600 °C, respectively. As a comparison, the undoped TiO_2 nanotubes were also synthesized via the same approach.

2.2. Photocatalytic performances of the Gd–La codoped TiO_2 nanotubes

The photodegradation reactions were carried out under atmospheric condition using 300 W ultraviolet lamps (PHILIPS 365 nm) as the irradiation sources at ambient conditions. A 420 nm cutoff filter with larger than 90% transmission was employed in order to obtain visible light. The irradiation distance between the lamp and the sample was 10 cm. 0.1 g of Gd–La codoped TiO_2 nanotubes were added into a cylindrical glass vessel containing 100 ml of RB aqueous solution with a concentration of 20 mg L^{-1}. Before exposing the sample to the light source, the RB aqueous solution was stirred thoroughly with the catalyst slide in the dark for 30 min to reach the adsorption equilibrium of the dye on the catalyst. At an interval of 10 min and ultraviolet irradiation, the photodegradation reaction was ceased and the solution was centrifuged. The residual dye concentration in the supernatant was measured by a UV–vis spectrometer (Lambda850) at maximum absorption wavelength of 552 nm for RB.

2.3. Characterizations

The morphology was observed using SEM equipped with energy dispersive spectroscopy (EDS) (JSM-2100F, JEOL) and a TEM (JEM2010, JEOL). The crystal structure of the as-prepared catalysts were characterized by an XRD (X'pert MPD Pro, Philips, The Netherlands with CuKα radiation ($\lambda = 0.15418$ nm) in the 2θ range from 5° to 80° operating at 40 kV accelerating voltage and 40 mA current). The optical absorption spectra were recorded on a UV–vis spectrophotometer (Agilent 8453) at room temperature. Fourier transformed Raman spectroscopic measurements in the ultraviolet light were performed on a Renishaw inVia Reflex Raman Spectrometer. High-resolution gratings were used to give a spectral resolution of 2 cm^{-1}. The spectra were recorded at room temperature from 1200 to 100 cm^{-1} using 16 scans with an exposure time of 1 s per scan. XPS experiments were carried out on a RBD upgraded PHI-5000C ESCA system (Perkin Elmer) with Mg Kα radiation ($h\nu = 1253.6$ eV). In general, the X-ray anode was run at 250 W and the high voltage was kept at 14.0 kV with a detection angle at 54°. The pass energy was fixed at 23.5, 46.95 or 93.90 eV to ensure sufficient resolution and sensitivity. The base pressure of the analyzer chamber was about 5×10^{-8} Pa. The sample was directly pressed to a self-supported disk (10×10 mm^2) and mounted on a sample holder then transferred into the analyzer chamber. Binding energies were calibrated by using the containment carbon (C1s = 284.6 eV).

3. Results and discussion

3.1. Morphology

The typical SEM image of uncalcined Gd–La codoped TiO_2 is shown in Fig. 1a. The uncalcined TiO_2 is in nanotubular morphology with an average diameter of 15∼20 nm, which can be validated by the TEM photograph in Fig. 1b. Close inspection of the TiO_2 nanotubes revealed that the rough surface was composed of the compactly aggregated and interpenetrated nanotubes, as shown in Fig. 1b. After calcining at 300, 400, and 500 °C (Fig. 1c–h), the similar morphology was observed without evident deviation, indicated that the nanotubular structure had no variation during the calcination procedure. However, the sample calcined at 600 °C (Fig. 1i and j) was composed of nanotubes and nanoparticles. It is believed that the formation of TiO_2 nanotubes is attributed to the curling of TiO_2 nanosheets via calcination at high temperatures due to the high-energy state [10]. No crystal lattice was found in all TEM images, suggesting that the crystallinity of Gd–La codoped TiO_2 nanotubes was not reasonable. The ionic radius of Ti^{4+}, La^{3+}, and Gd^{3+} are 0.068, 0.115, and 0.0938 nm, respectively [11]. Due to the fact that the radius of Ti^{4+} is much less than that of La^{3+} and Gd^{3+}, Ti^{4+} could enter the La^{3+} and Gd^{3+} lattices during synthesis [10], leading to a great deal of lattice distortions and plenty of defects at and under surface of Gd–La codoped TiO_2 nanotubes.

3.2. Structure

The crystal phase of the resultant Gd–La codoped TiO_2 nanotubes was identified by XRD, as shown in Fig. 2. The diffraction peaks at $2\theta = 25.4°$, 37.8°, 48.1°, 53.9°, 62.7° and 68.8°in the spectrum of Gd–La codoped TiO_2 nanotubes were identified and attributed to the diffraction faces of (101), (103), (200), (105), (204) and (116), respectively, showing the crystal phase of anatase (Fig. 2). The peak intensity of (101) phase was enhanced by elevating calcining temperature. Compared with undoped TiO_2 nanotubes, the crystallinity of TiO_2 was decreased by doping rare earth oxides, which is consistent with the result in Nd doped TiO_2 nanotubes [10]. Interestingly, new diffraction peaks belonging to $La_xTi_yO_z$ and $Gd_xTi_yO_z$ were generated ranging from 27° to 34° after calcining at 300 °C.

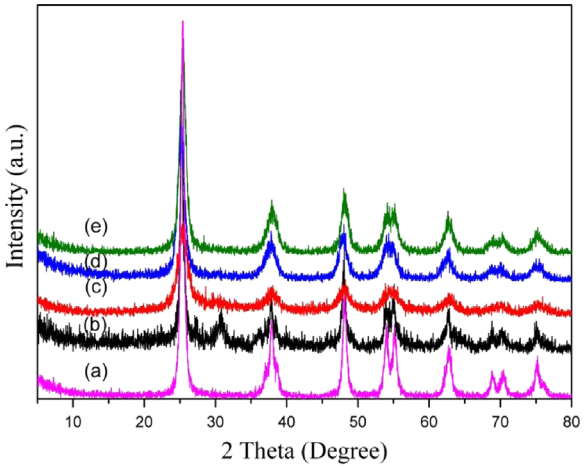

Fig. 2. XRD patterns of (a) uncalcined Gd–La codoped TiO_2 nanotubes, and Gd–La codoped TiO_2 nanotubes calcined at (b) 300 °C, (c) 400 °C, (d) 500 °C, and (e) 600 °C.

Table 1
Cell parameters of the undoped and Gd–La codoped TiO_2 nanotubes.

	a/*b* (Å)	*c* (Å)
Undoped	3.77068	9.4768
300 °C	3.76763	9.47995
400 °C	3.78733	9.48118
500 °C	3.79039	9.5139
600 °C	3.7852	9.47553

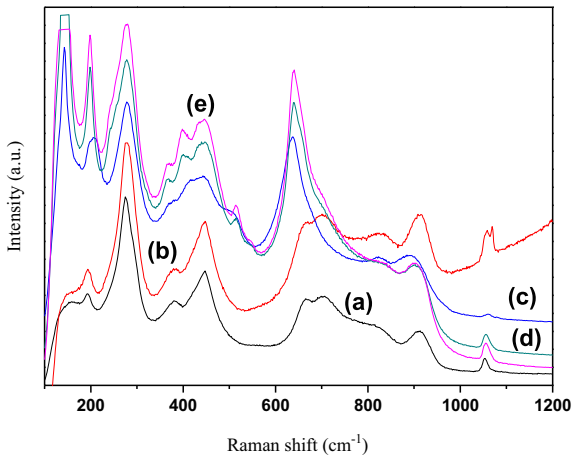

Fig. 3. Raman spectra of (a) uncalcined Gd–La codoped TiO_2 nanotubes, and Gd–La codoped TiO_2 nanotubes calcined at (b) 300 °C, (c) 400 °C, (d) 500 °C, and (e) 600 °C.

However, when the calcination temperature increased to 400 °C, $La_xTi_yO_z$ and $Gd_xTi_yO_z$ were not stable and may be changed into rare earth dioxide. No diffraction peaks of rare earth oxides were detected in the XRD patterns, due to the content of rare earth oxides being possibly below the detection limit of XRD analysis and to the large difference between the ionic radii of Ti^{4+} and lanthanide ions (La^{3+} and Gd^{3+}) [12]. Moreover, there is a slight difference in the lattice parameters "*a*" and "*c*" (Table 1) between undoped and Gd–La codoped TiO_2 photocatalysts, which indicates that the Ti^{4+} enters the lattice of rare earth oxide and induces lattice distortion [13]. With the increasing of temperature, the cell parameters increase first and then decrease after reaching the temperature of 500 °C.

Crystallographic structure of the calcined Gd–La codoped TiO_2 nanotubes was judged by Raman spectroscopy and shown in Fig. 3. As a comparison, the Raman spectrum of the uncalcined Gd–La codoped TiO_2 nanotubes was also conducted. The Raman bands at 142.9, 199.9, 398.1, 515.1, and 640.6 cm^{-1} in the Gd–La codoped TiO_2 nanotubes calcined at 600 °C are attributed to E_g, B_{1g}, A_{1g}, B_{2g}, and E_g modes of anatase phase of TiO_2 (Table 2), respectively. The result is consistent with that of XRD analysis. Besides these peaks, some additional peaks around 195, 278, 446, 900, and 1055 cm^{-1}, attributing to Gd_2O_3 and La_2O_3, were observed in the Raman spectra of the Gd–La codoped TiO_2 nanotubes. The detection of doped rare earth oxides in TiO_2 has also been reported in the literature [14]. Furthermore, the mode positions have shifted compared to uncalcined TiO_2 nanotubes, which could be attributed to the deviation in crystallite size and lack of adjacent atoms for the surface atoms because of the substitution of La^{3+} and Gd^{3+} lattices by Ti^{4+} during synthesis. Therefore, the surface atoms are in a relaxation state and the band shift results from a surface relaxation effect [15].

In order to describe the photo-absorption behavior of the calcined Gd–La codoped TiO_2 nanotubes, the UV–vis diffuse reflection spectrum was recorded and shown in Fig. 4. The absorption spectrum of uncalcined TiO_2 nanotubes was also conducted for comparison. No obvious shape alteration was observed via high-temperature calcination. Uncalcined Gd–La codoped TiO_2 nanotubes and the nanotubes calcined at 300 and 400 °C exhibited absorption in visible light region, and its absorption edge was around 450–500 nm, which was consistent with the reference [16]. However, the absorption edges of the Gd–La codoped TiO_2 nanotubes calcined at 500 and 600 °C were positioned at 400–450 nm. The blue shift, attributing to the quantum size effect [17], was detected in the spectra of high-temperature calcined TiO_2 nanotubes compared with our previous report [11], suggesting that the codoping of Gd–La did not give rise to new spectrum phenomena as well as could inhibit the growth of anatase crystallite. The results were in good agreement with the XRD analysis.

The charge imbalance caused by Ti^{4+} replacing La^{3+} and Gd^{3+} to enter into the lattices of La_2O_3 and Gd_2O_3 reduces Ti^{4+} to Ti^{3+}, as well as the electron transfer from La or Gd to Ti in the Ti–O–La or Ti–O–Gd bonds because of the lower Pauling electronegativity values of La (1.1) and Gd (1.2) than Ti (1.5), which makes Ti more electron rich and can be validated by the shift of $Ti2p_{3/2}$ peak from 458.9 eV in undoped TiO_2 to 457.9 eV in uncalcined Gd–La codoped TiO_2 nanotubes (Fig. 5) [18]. The peak position at 529.5 eV in uncalcined Gd–La codoped TiO_2 means the presence of Ti_2O_3 [19]. The detection of La3d and Gd4d peaks at 833.1 and 143.6 eV indicates the codoping of La_2O_3 and Gd_2O_3. However, the peak shifts of La3d and Gd4d from 833.1 eV and 143.6 eV at uncalcined Gd–La codoped TiO_2 nanotubes to 838.4 eV and 140.4 eV at the codoped TiO_2 nanotubes calcined at 500 °C may result from the increased bonding during calcination process.

3.3. Photocatalytic performances

Fig. 6 shows the time course of the decrease in the concentration of RB. Under visible-light irradiation, RB molecules were photodegraded very slowly by uncalcined TiO_2 nanotubes due to their low photosensitization. The photocatalytic activities of the Gd–La codoped TiO_2 nanotubes calcined at various temperatures were also depicted as references to evaluate the activity of the codoped TiO_2, showing a significant enhancement in photocatalytic activity. It was found that the Gd–La codoped TiO_2 nanotubes calcined at 500 °C presented the highest photocatalytic activity. Nearly all the RB molecules were exhausted after irradiation of 220 min, whereas

Table 2
Assignments of Raman bands (cm^{-1}) of the Gd–La codoped TiO_2 nanotubes.

Uncalcined	300 °C	400 °C	500 °C	600 °C	Modes
155.9	155.8	142.9	142.9	142.9	E_g
194.0	194.0	200.1	199.9	199.9	B_{1g}
383.4	383.4	380.4	398.1	398.1	A_{1g}
–	–	–	515.1	515.1	B_{2g}
668.6	668.6	634.6	640.6	640.6	E_g

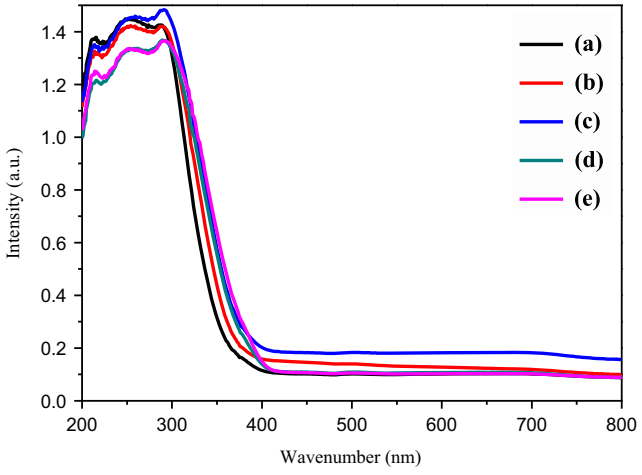

Fig. 4. UV–vis diffuse reflection spectra of (a) uncalcined Gd–La codoped TiO_2 nanotubes, and Gd–La codoped TiO_2 nanotubes calcined at (b) 300 °C, (c) 400 °C, (d) 500 °C, and (e) 600 °C.

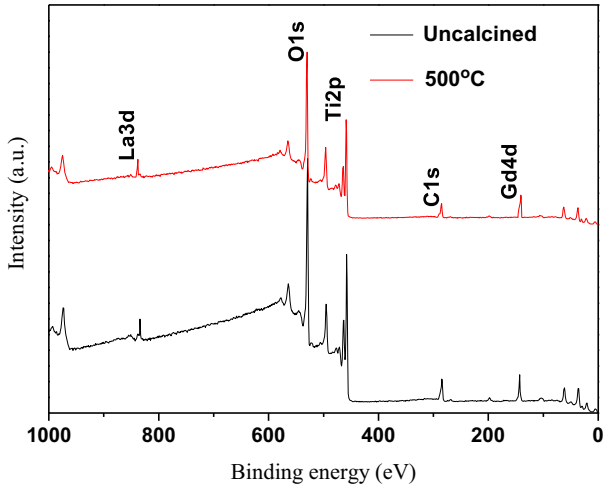

Fig. 5. XPS survey spectra for uncalcined Gd–La codoped TiO_2 nanotubes, and Gd–La codoped TiO_2 nanotubes calcined at 500 °C.

the photodegradation rate of RB by uncalcined TiO_2 nanotubes was only 20% at the same time. The significant enhancement in photocatalytic activity could be attributed to the excitation of calcined Gd–La codoped TiO_2 nanotubes under the irradiation of visible-light, therefore, more electron–hole pairs were produced.

The kinetics of the photodegradation of RB in the presence of the uncalcined and Gd–La codoped TiO_2 nanotubes were also studied. The $-\ln(C/C_0)$ of these samples present good linear relation with the irradiation time (shown in Fig. 6b), which means that the photodegradation of RB obeys the rules of the first-order reaction kinetics $-\ln(C/C_0)=kt$ [20]. The reaction rate constants k of the photodegradation of RB from Gd–La codoped TiO_2 nanotubes calcined at 500 °C was the highest, indicating a best visible-light photocatalyst.

The Gd–La codoped TiO_2 nanotubes calcined at 500 °C show the best photocatalytic activity, because of the highest quantity of surface defects and oxygen vacancies. The abundant surface defects provide numerous active sites for dye adsorption, whereas the oxygen vacancies are traps to electrons which result in an efficient separation of photogenerated electron–hole pairs. The decoration of TiO_2 by oxygen vacancies results in a shortened distance for electron transport, making oxygen vacancies easily bind electrons to form excitations and formation of an excitation energy level near the bottom of the conduction band (Fig. 7) [21]. The decrease of the bandgap between the excitation energy level and valence band of TiO_2 dramatically increases the electron–hole excitation and number.

4. Conclusions

In summary, we have demonstrated the fabrication of Gd–La codoped TiO_2 nanoparticles for high-efficient visible-light photocatalysts. Photocatalytic degradation of RB revealed that Gd–La codoped TiO_2 nanotubes calcined 500 °C can work more efficiently as visible-light photocatalysts comparing with the uncalcined or calcined TiO_2 nanotubes at other temperatures. Ti^{4+} substitute for La^{3+} and Gd^{3+} in the crystal lattices of La_2O_3 and Gd_2O_3 to create abundant oxygen vacancies and surface defects. The oxygen vacancies can easily bind electrons to form an excitation energy level below the conduction band of TiO_2 nanotubes, resulting in an efficiently photocatalytic activity under visible-light irradiation. Moreover, the surface defects provide active sites to adsorb RB molecules which shortens the transfer distance of photogenerated charges. A preliminary research on photocatalytic performances reveals a significant enhancement in the photodegradation of RB under visible-light irradiation by Gd–La codoping and obeys the rules of the first-order reaction kinetics. The insight into the effect of lower excitation energy on charge separation and excitation was proposed, providing a promising platform for fabricating highly efficient visible-light photocatalysts or anodes for photovoltaic cells.

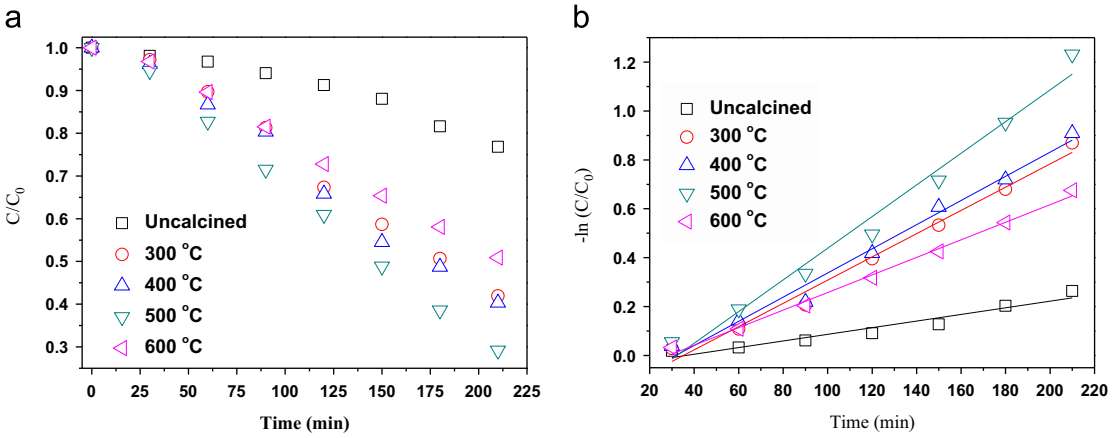

Fig. 6. (a) Time course of the decrease in the concentration for the photodegradation of RB and (b) relationships between ln (C/C_0) and time by uncalcined and calcined Gd–La codoped TiO_2 nanotubes.

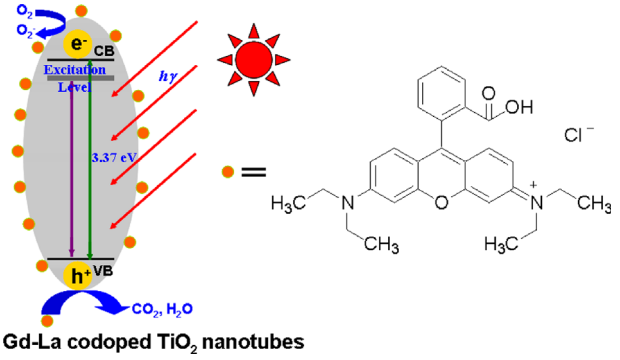

Fig. 7. Schematic of the photodegradation of RB in the Gd–La codoped TiO_2 nanotubes.

Acknowledgments

This work was supported by the Shanghai Committee of Science and Technology (12nm0504800), the Minhang District Science and Technology Project of Shanghai (2012MH017), the Shanghai Committee of Science and Technology (13ZR1429300), the National Nature Science Foundations of China (21071098), and the International Science and technology Cooperation Project of Shanghai (11520706100).

References

[1] M.N. An'amt, S. Radiman, N.M. Huang, M.A. Yarmo, N.P. Ariyanto, H.N. Lim, M.R. Muhamad, Sol–gel hydrothermal synthesis of bismuth–TiO_2 nanocubes for dye-sensitized solar cell, Ceram. Int. 36 (2010) 2215–2220.

[2] Q.W. Tang, L. Lin, X. Zhao, K. Huang, J.H. Wu, p–n Heterojunction on ordered ZnO nanowires/polyaniline, Langmuir 28 (2012) 3972–3978.

[3] T.X. Fan, S.K. Chow, D. Zhang, Biomorphic mineralization: from biology to materials, Prog. Mater. Sci. 54 (2009) 542–659.

[4] J.Y. He, W.M. Wang, F. Long, Z.G. Zou, Z.Y. Fu, Z. Xu, Hydrothermal synthesis of hierarchical rose-like Bi_2WO_6 microspheres with high photocatalytic activities under visible-light irradiation, Mater. Sci. Eng. B 177 (2012) 967–974.

[5] I. Tacchini, A. Anson-Casaos, Y. Yu, M.T. Martinez, M. Lira-Cantu, Hydrothermal synthesis of 1D TiO_2 nanostructures for dye sensitized solar cells, Mater. Sci. Eng. B 177 (2012) 19–26.

[6] R. Asahi, T. Morikawa, T. Ohwaki, K. Aoki, Y. Taga, Visible-light photocatalysis in nitrogen-doped titanium oxides, Science 293 (2001) 269–271.

[7] N.R. Khalid, E. Ahmed, Z.L. Hong, Y.W. Zhang, M. Ullah, M. Ahmed, Graphene modified Nd/TiO_2 photocatalyst for methyl orange degradation under visible light irradiation, Ceram. Int. 39 (2013) 3569–3575.

[8] Z.X. Li, F.B. Shi, T. Zhang, H.S. Wu, L.D. Sun, C.H. Yan, Stabilized ordered mesoporous titania for near-infrared photocatalysis, Chem. Commun. 47 (2011) 8109–8111.

[9] Z.M. El-Bahy, A.A. Ismail, R.M. Mohamed, Enhancement of titania by doping rare earth for photodegradation of organic dye (Direct Blue), J. Hazard. Mater. 166 (2009) 138–143.

[10] Y.H. Xu, C. Chen, X.L. Yang, X. Li, B.F. Wang, Preparation characterization and photocatalytic activity of the neodymium doped TiO_2 nanotubes, Appl. Surf. Sci. 255 (2009) 8624–8628.

[11] L. Lin, Y.C. Yang, X. Wang, D.N. He, Q.W. Tang, S. Ghoshroy, Hierarchical Gd–La codoped TiO_2 microspheres as robust photocatalysts, Int. J. Hydrog. Energy 38 (2013) 2634–2640.

[12] H.X. Shi, T.Y. Zhang, T.C. An, B. Li, X. Wang, Enhancement of photocatalytic activity of nano-scale TiO_2 particles co-doped by rare earth elements and heteropolyacids, J. Colloid Interface Sci. 380 (2012) 121–127.

[13] F.B. Li, X.Z. Li, M.F. Hou, Photocatalytic degradation of 2-mercaptobenzothiazole in aqueous La^{3+}–TiO_2 suspension for odor control, Appl. Catal. B—Environ. 48 (2004) 185–194.

[14] E.J. Wang, W.S. Yang, Y.A. Cao, Unique surface chemical species on indium doped TiO_2 and their effect on the visible light photocatalytic activity, J. Phys. Chem. C 113 (2009) 20912–20917.

[15] C.H. Yang, Z.Q. Ma, F. Li, B. He, J.H. Yuan, Z.H. Zhang, Spectrum Analysis on Phase Transformations in TiO_2 Thin Films, Acta Phys.-Chim. Sin. 26 (2010) 1349–1354.

[16] K. Chen, J.Y. Li, J. Li, Y.M. Zhang, W.X. Wang, Physicochemical engineering aspects, Colloid Surf. A 360 (2010) 47–56.

[17] L.Q. Jing, X.J. Sun, B.F. Xin, B.Q. Wang, W.M. Cai, H.G. Fu, The preparation and characterization of La doped TiO_2 nanoparticles and their photocatalytic activity, J. Solid State Chem. 177 (2004) 3375–3382.

[18] B.M. Reddy, B. Chowdhury, P.G. Smirniotis, An XPS study of La_2O_3 and In_2O_3 influence on the physicochemical properties of MoO_3/TiO_2 catalysts, Appl. Catal. A: Gen. 219 (2001) 53–60.

[19] F.B. Li, X.Z. Li, M.F. Hou, Photocatalytic degradation of 2-mercaptobenzothiazole in aqueous La^{3+}–TiO_2 suspension for odor control, Appl. Catal. B—Environ. 48 (2004) 185–194.

[20] D. Wang, Y. Duan, Q. Luo, X. Li, L. Bao, Desalination of Iraqi surface water using nanofiltration membranes, Desalination 270 (2011) 174–180.

[21] L.D. Zhang, J.M. Mou, Nanomaterials and Nanostructure, Science Press, Beijing, 2001, p. 312–313.